

Article

Effect of Cobalt Substitution on the Structural and Magnetic Properties of Bismuth Ferrite Powders

Hector A. Chinchay-Espino ^{1,*}, Gina M. Montes-Albino ², Carlex M. Morales-Cruz ³, Segundo E. Dobbertin-Sanchez ⁴ and Segundo Rojas-Flores ⁵

¹ Departamento de Ciencias, Universidad Privada del Norte, Chorrillos, Lima 15054, Peru

² Department of Mechanical Engineering, University of Puerto Rico, Mayaguez Campus, Mayaguez, PR 00682, USA; gina.montes@upr.edu

³ Department of Chemical Engineering, University of Puerto Rico, Mayaguez Campus, Mayaguez, PR 00682, USA; carlex.morales@upr.edu

⁴ Departamento de Ciencias, Universidad Privada del Norte, Cajamarca 06002, Peru; segundo.dobbertin@upn.edu.pe

⁵ Escuela de Ingeniería Mecánica Eléctrica, Universidad Señor de Sipán, Chiclayo 14000, Peru; segundo.rojas.89@gmail.com

* Correspondence: hector.chinchay@upn.edu.pe

Abstract: BiFeO₃ (BFO) is a multiferroic material with excellent ferroelectric properties but with poor magnetic behavior. Therefore, we focused principally on the enhancement of the magnetic order of BFO. These multiferroic properties make BFO an excellent candidate for magnetoelectric devices at room temperature. Pure and Co-BiFeO₃ powders were successfully synthesized via the sol-gel method at 700 °C. The effect of Co substitution on the corresponding structural and magnetic properties of BFO was studied. X-ray diffraction and Fourier Transform Infrared Spectroscopy measurements confirmed the rhombohedral perovskite structure in all samples. A secondary phase of CoFe₂O₄ (CFO) was detected for 9, 10, and 15% of Co doping. The scanning electron microscopy images of the Co-BFO particles showed a reduction in the particle size compared to the pure BFO powders. Vibrating sample magnetometry measurements evidenced the ferromagnetic hysteresis loop for the Co-BFO powders with values of saturation magnetization of 4.1 emu/g and a coercivity of 1083 Oe for 15% of Co doping. In this work, we report impurity free samples with notable magnetic properties at the same time, which is a difficult challenge in bismuth ferrite synthesis. This is the first step for later applications in future technology.

Keywords: multiferroic; sol-gel; magnetic property; bismuth ferrite; cobalt ferrite



Citation: Chinchay-Espino, H.A.; Montes-Albino, G.M.; Morales-Cruz, C.M.; Dobbertin-Sanchez, S.E.; Rojas-Flores, S. Effect of Cobalt Substitution on the Structural and Magnetic Properties of Bismuth Ferrite Powders. *Crystals* **2022**, *12*, 1058. <https://doi.org/10.3390/cryst12081058>

Academic Editor: Artem Pronin

Received: 30 June 2022

Accepted: 26 July 2022

Published: 29 July 2022

Publisher's Note: MDPI stays neutral with regard to jurisdictional claims in published maps and institutional affiliations.



Copyright: © 2022 by the authors. Licensee MDPI, Basel, Switzerland. This article is an open access article distributed under the terms and conditions of the Creative Commons Attribution (CC BY) license (<https://creativecommons.org/licenses/by/4.0/>).

1. Introduction

Multiferroic materials have attracted interest from researchers due to their expected spontaneous and switchable ferroelectric, ferromagnetic, and ferroelastic ordering in a single phase. Furthermore, tuning of the magnetic and electric properties can be attained using a magnetic and electric field, respectively, and through electromagnetic coupling. In other words, an external electric field can induce a magnetic response and an external magnetic field can modify the electric polarization in the same material [1]. Among multiferroics, Bismuth Ferrite (BFO) is one of the most important materials exhibiting multifunctional properties at room temperature. BFO is ferroelectric with a Curie temperature of $T_C \sim 1103$ K and a G-type antiferromagnetic ordering with a Neel temperature of $T_N \sim 643$ K [2]. These features make BFO a good candidate for applications in electronic devices, data storage, sensors, and spintronics [3–8]. Moreover, BFO shows a weak magnetism due its spiral spin structure, which makes doping a promising route to enhance its magnetic properties. This incorporation of dopant species can induce a distortion in the BFO unit cell due to the mismatch between the ionic radius of the host and guest atoms

that will change the Fe-O-Fe bond angles and, according to the Goodenough–Kanamori rule, switch the magnetic ordering [9]. Costa et al. [10] improved the magnetic properties by doping BiFeO₃ with Ca in Bi sites. Other dopants, such as Mn, Co, and Ni, have also been considered in an attempt to enhance the corresponding magnetic properties [11–13]. In particular, the synthesis of Co-BiFeO₃ nanocrystalline powders involved the presence of Cobalt Ferrite (CFO) as a secondary phase [14]. CFO is a ferromagnetic material that opens the possibility to form BiFeO₃/CoFe₂O₄ nanocomposites, which would combine ferroelectric and ferromagnetic features.

On a general basis, several approaches have been used to synthesize BFO powders, e.g., hydrothermal [15], sol–gel [16], solid state [17], and co-precipitation [18], among others. Sol–gel is a rapid and simple synthesis method that also allows a good control of crystallite size and composition. The preparation of impurity-free BFO is a current challenge, since the scientific literature reports the coexistence of Bi₂₅FeO₃₉ [19] and Bi₂Fe₄O₉ [10]. Selective dissolution, so-called leaching, is an alternative to remove these secondary phases [20], at the expense of prolonging the processing time and generating unwanted liquid waste.

In the present work, we investigated the effect of Co substitution in impurity-free BFO on the structural and magnetic properties of the powders synthesized via a modified sol-gel approach. Depending on the Co doping level, CFO was detected in coexistence with pure BFO; it explained the observed enhancement in the ferromagnetic behavior of the as-synthesized nanocrystalline powders.

2. Materials and Methods

2.1. Materials

All reagents were of analytical grade and used without any further purification. Bismuth nitrate [Bi(NO₃)₃·5H₂O, 99.9% Alfa Aesar, Massachusetts, MA, USA], iron nitrate [Fe(NO₃)₃·9H₂O, 99.9% Alfa Aesar], and cobalt (II) acetate tetrahydrate [Co(CH₃COO)₂·4H₂O, 98%, Alfa Aesar] were used as the precursor salts, whereas ethylene glycol [EG, HOCH₂CH₂OH, 99% Alfa Aesar] was used as the solvent.

2.2. Synthesis of Pure and Co-BFO Powders

Well-crystallized BiFeO₃ nanocrystalline powders were synthesized via a modified sol–gel and thermal treatment method. Suitable amounts of Bi, Fe, and Co salts were used to achieve the desired atomic fractions of Bi_(1-x)Co_xFeO₃, with x = 0, 0.05, 0.06, 0.07, 0.08, 0.09, 0.10, and 0.15. Precursor salts were dissolved in ethylene glycol at 150 °C, followed by drying at 350 °C and milling. The obtained solid precursor was then thermally annealed in air for 30 min at 700 °C to develop the desired crystalline structure in agreement with the temperature conditions used in a previous work [12]. The heating rate was 5 °C/min for all these experiments.

2.3. Materials Characterization

The crystalline structure of the as-synthesized powders was studied by X-ray diffraction (XRD) using a SIEMENS D 500 diffractometer with a Cu-K α radiation. The morphology and size of the particles were studied in a JEOL scanning electron microscope. Fourier Transform Infrared Spectroscopy (FTIR) was used to identify structural features and investigate the chemical structure of produced samples. The corresponding magnetic properties were measured at room temperature in a Lake Shore 7410 vibrating sample magnetometer (VSM).

3. Results and Discussion

3.1. XRD Analysis

Figure 1 shows the XRD patterns for Bi_(1-x)Co_xFeO₃ (x = 0, 0.05, 0.06, 0.07, 0.08, 0.09, 0.10, and 0.15) powders thermally treated at 700 °C for 30 min. Match software verified that all main peaks corresponded to the rhombohedral perovskite structure of BFO. For 0 and 5 at.% of Co doping, the main impurity phases of Bi₂Fe₄O₉ (mullite) or Bi₂₅FeO₃₉ (sillénite)

were detected in the 25° – 30° diffraction angle range. The presence of these intermediate oxides can be attributed to the thermal decomposition of the initially generated BFO or incomplete transition of precursors into BFO [20]. No peaks coming from any impurities were detected for 8, 9, 10, and 15 at.% of Co doping. Instead, a secondary phase of cobalt ferrite (CFO) was identified as evidenced by the appearance of a peak at $\sim 35.4^{\circ}$ that belonged to the cubic spinel structure of CFO [21]. The Co (II) species would have reacted with the available Fe (III) species to form CFO, which also inhibited the formation of impurities: the Fe species were no longer available for the formation of Bi-Fe impurity phases. The presence of cobalt ferrite in Co-doped BiFeO_3 powders has been reported by other researchers but coexisting with a large amount of impurities [14].

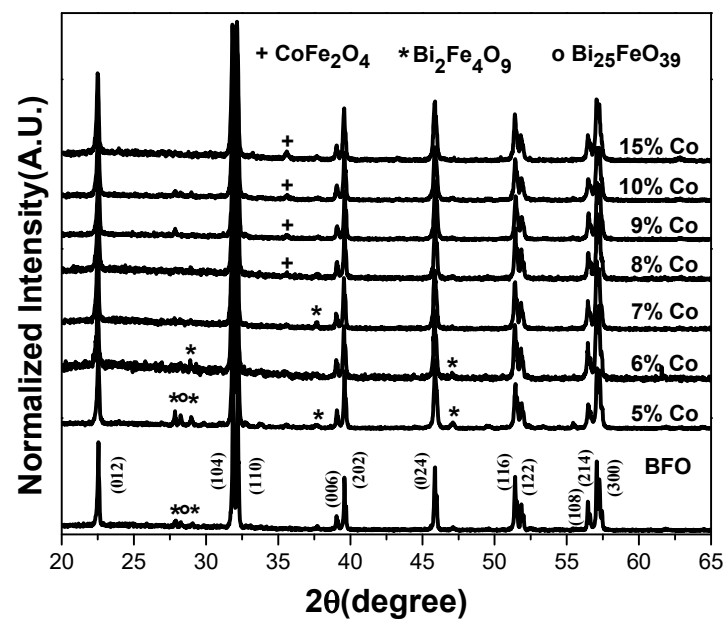


Figure 1. XRD patterns for Co-doped BFO powders thermally treated at 700°C for 30 min.

Incorporation of Co species in Bi sites should give place to a shrinking in the unit cell due to the mismatch in ionic radii between Co^{2+} (0.78 \AA) and Bi^{3+} (1.20 \AA); consequently, the diffraction peaks of Co-doped BFO were expected to be shifted toward higher diffraction angles with respect to the peaks for pure BFO powders. However, as Figure 2 suggests for the (012) peak, a shift toward lower diffraction angles with doping (particularly in the Co doping range of 5 to 7 at.%), was observed. This trend may suggest an expansion of the unit cell due to the incorporation of Co^{2+} (0.78 \AA) in the Fe^{3+} (0.64 \AA) sites, instead. For 8 and 9 at.% of Co, the shift was not so evident because the formation of CFO should have been the dominant mechanism rather than substitution of Fe species by Co sites. At higher compositions of Co (10 and 15%), both mechanisms would have become evident, i.e., the initial substitution of Fe by Co species and the chemical reaction between Fe and Co to form the CFO phase.

The volume of the unit cell at each doping level was determined as an attempt to corroborate the mechanisms proposed in the incorporation of Co and the formation of CFO (Figure 3). From 5 to 7 at.% of Co, an increase in the volume of the unit cell was observed (incorporation of Co^{2+} in Fe^{3+} sites); for 8 and 9 at.% of Co, the volume remained almost constant (prevailed formation of CFO rather than the incorporation of Co^{2+}). Finally, for 10 and 15 at.% of Co, an expansion of the volume of unit cell was observed. This expansion in the unit cell took place with the simultaneous detection of the CFO phase by XRD analysis.

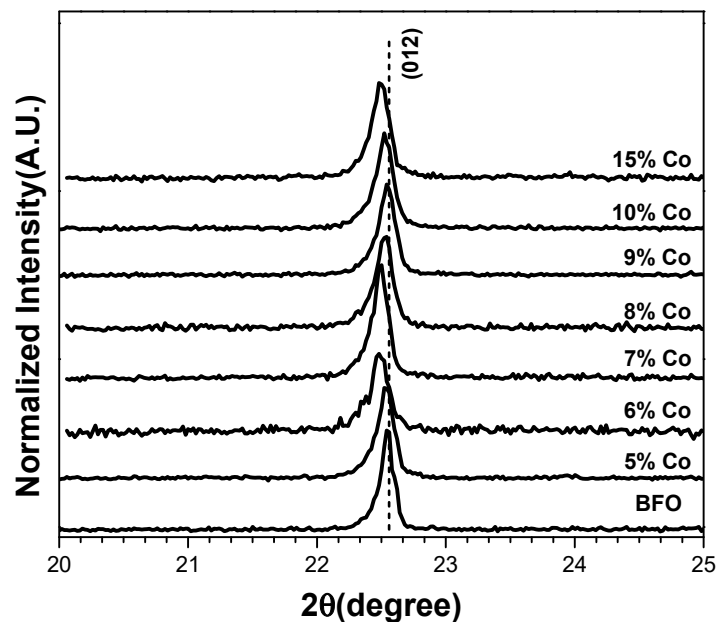


Figure 2. Detail of (012) peak shift for Co-doped BFO powders thermally treated at 700 °C for 30 min.

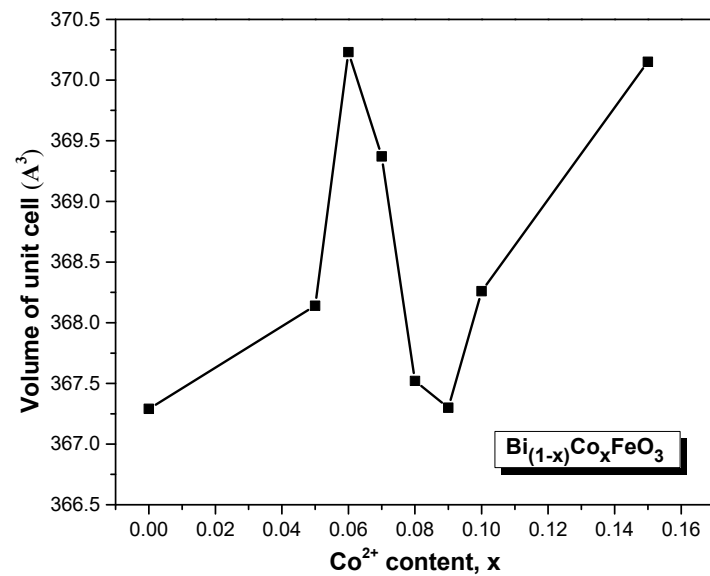


Figure 3. Effect of Co^{2+} ions content on the volume of unit cell of BiFeO_3 powders thermally annealed at 700 °C for 30 min.

3.2. FTIR Analysis

Figure 4 shows the room temperature FTIR spectra of the Co-doped BFO samples synthesized at different levels of doping. The band at 813 cm^{-1} corresponded to the Fe-O stretching vibration, which only was detected for pure and 5% Co-doped BFO powders. Other bands were detected at 539 cm^{-1} (pure BFO) and 550 cm^{-1} (15% Co-doped BFO) and can be attributed to the Fe-O bending vibration in the BFO host lattice. The Fe-O band is attributed to the perovskite structure [22,23]. The shift in this band with the doping level reveals a distortion in the octahedral FeO_6 groups.

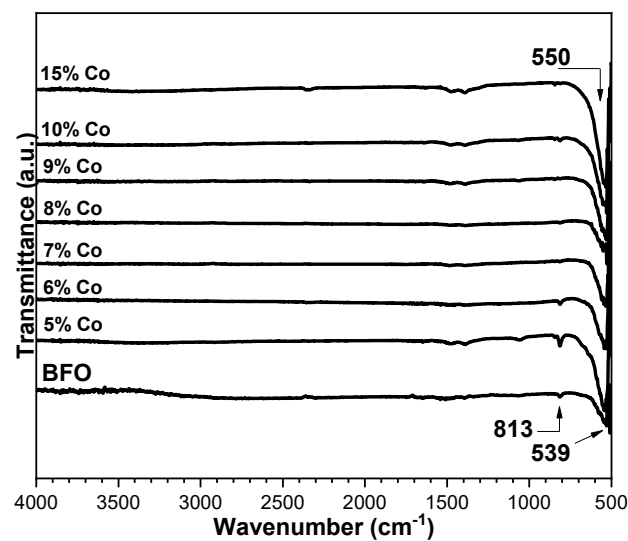


Figure 4. FTIR spectra of Co-doped BiFeO₃ powders synthesized at different levels of Co doping.

3.3. Scanning Electron Microscopy (SEM) Analysis

Figure 5 shows the SEM images corresponding to 0% and 15% Co-doped BFO powders. Pure BFO powders consist of highly agglomerated particles with an irregular shape. The average particle size was estimated by ImageJ software at $\sim 1.20 \mu\text{m}$. In turn, the SEM image for the Co(15%)-BFO powders clearly evidenced less agglomeration, a smaller particle size (average size estimated at 240 nm), and a high monodispersity. The decrease in the particle size was attributed to the incorporation of the Co species in the host BFO. Therefore, this can be explained by an increase in the nucleation rate due to lattice distortions induced by the difference in the ionic radius between Bi³⁺ and the dopant [24].

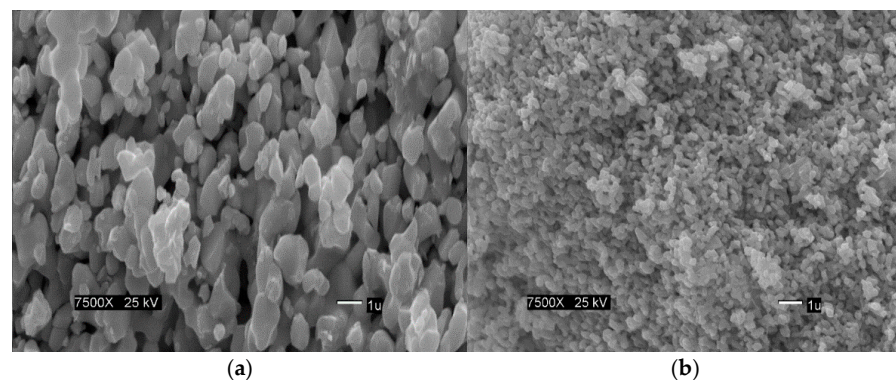


Figure 5. SEM micrographs of (a) pure and (b) 15% Co-doped BiFeO₃ powders thermally treated at 700 °C for 30 min.

3.4. M-H Measurements

Figure 6 shows the magnetic hysteresis loop measured at room temperature for the Co-doped BiFeO₃ powders. All Co-doped BFO samples exhibited a well-saturated ferromagnetic hysteresis loop, contrasting with the pure BFO that displayed a M-H dependence typical of a material with an antiferromagnetic ordering. As suggested before, the incorporation of Co²⁺ ions in the Fe³⁺ sites could be considered as the predominant mechanisms for 5–7% at.% of Co doping that would have induced changes in the Fe-O-Fe bond angles and, hence, negatively affected the antiferromagnetic ordering. In turn, the enhancement in the magnetic properties for the Co-doped BFO was attributed to the formation of the ferromagnetic cobalt ferrite at higher doping levels. The changes in Fe-O-Fe bond angles, induced by substitution of Fe by Co species, should have also been involved with the enhancement on magnetization in those Co-doped BFO samples.

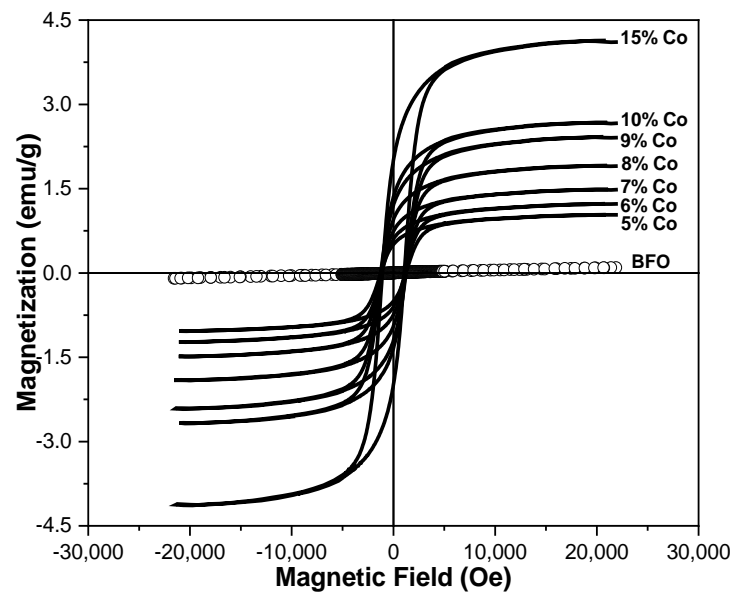


Figure 6. Magnetic hysteresis loop for Co-doped BiFeO_3 powders synthesized at different levels of Co-doping.

Figure 7 summarizes the variation of the remnant and saturation magnetization with the doping level. As said before, this trend was attributed to distortions in the Fe-O-Fe bond angles and the ferromagnetic ordering provided by the co-existing cobalt ferrite. The reduction in the particle size in the doped samples (as evidenced by SEM images) would modify the spiral spin structure of the non-doped BFO that could also induce ferromagnetic ordering. [23,25–27]. In our case, the 15% Co-doped BFO powders exhibited a maximum saturation magnetization (4.1 emu/g) that was 43 times higher than that of non-doped BFO (Table 1). Furthermore, the coercivity was drastically enhanced from 14.1 Oe up to 1083 Oe, for the pure and Co-BFO phases. These result trends in the magnetic properties can be attributed to the presence of Cobalt ferrite, in good agreement with those observations from Tang et al. [14]. However, Tang reported the synthesis of samples with a high impurity level and the presence of cobalt ferrite only for 20 and 25% of Co doping. In the present work, the presence of impurity phases was completely inhibited, and the formation of cobalt ferrite was detected for Co doping levels as low as 8% Co.

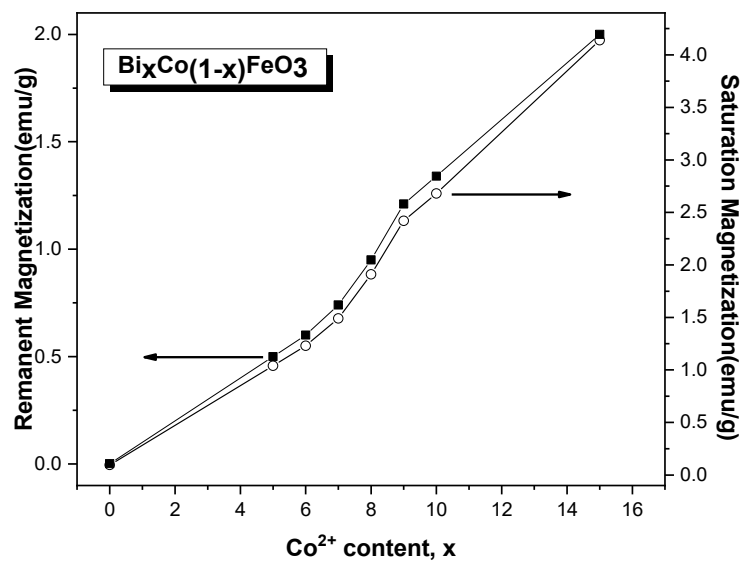


Figure 7. Variation in the magnetic parameters with Co^{2+} content, x , for $\text{Bi}_{(1-x)}\text{Co}_x\text{FeO}_3$, thermally treated at 700°C for 30 min.

Table 1. Magnetic parameters for the pure and 15% Co-doped BFO powders thermally treated at 700 °C for 30 min.

| Samples | Coercivity (Oe) | Saturation Magnetization (emu/g) |
|------------------|-----------------|----------------------------------|
| pure BFO | 14.1 | 0.1 |
| 15% Co-doped BFO | 1083 | 4.1 |

4. Conclusions

In summary, pure and Co-doped BiFeO₃ powders were well synthesized with the sol–gel method. XRD and FTIR analysis confirmed the formation of Co-doped BiFeO₃ powders with rhombohedral perovskite structure. The formation of cobalt ferrite in Co-doped BiFeO₃ powders inhibited the formation of impurities; Fe species would have been consumed to form the cobalt ferrite phase rather than become available to stabilize the Bi-Fe impurities. SEM images showed a particle size of 1.20 μm for the pure BFO and a decrease to 250 nm for the 15% Co-doped BFO. This reduction in particle size was attributed to the mismatch in the ionic radius between Bi³⁺ and Co²⁺. All the doped samples exhibited ferromagnetic behavior. The optimal doping condition was obtained for 15% Co-doped BFO with high values of saturation magnetization and a coercivity of 4.1 emu/g and 1083 Oe, respectively. The magnetization values were increased as the Co-content increased probably due to the distortion of the Fe–O–Fe bond angles and the presence of ferromagnetic cobalt ferrite coexisting with the BiFeO₃ host lattice. Otherwise, a balance between the electrical and magnetic properties of the Co-doped BiFeO₃ should be investigated for future applications in spintronics and memory devices.

Author Contributions: Conceptualization, H.A.C.-E. and G.M.M.-A.; methodology, H.A.C.-E.; validation, H.A.C.-E.; formal analysis, H.A.C.-E., C.M.M.-C. and S.E.D.-S.; investigation, C.M.M.-C. and S.E.D.-S.; resources, H.A.C.-E.; data curation, H.A.C.-E., S.E.D.-S. and S.R.-F.; writing—original draft preparation, H.A.C.-E.; writing—review and editing, S.R.-F., C.M.M.-C. and S.E.D.-S.; visualization, S.R.-F.; supervision, S.R.-F.; project administration, C.M.M.-C. and S.E.D.-S. All authors have read and agreed to the published version of the manuscript.

Funding: This project was partially supported by PR NASA Space Grant Consortium/EPSCoR (PR NASA Summer Internship Program).

Institutional Review Board Statement: Not applicable.

Informed Consent Statement: Not applicable.

Data Availability Statement: Not applicable.

Acknowledgments: (H Ch) would like to express his gratitude and appreciation for Oscar Perales for his mentorship through the development of this research project. The authors also extend their gratitude to Christian Villa (Graduate Student, University of Puerto Rico, Mayaguez Campus) for his support in the characterization of the samples.

Conflicts of Interest: The authors declare no conflict of interest.

References

- Spaldin, N.; Cheong, S.; Ramesh, R. Multiferroics: Past, present, and future. *Phys. Today* **2010**, *63*, 38. [[CrossRef](#)]
- Reddy, V.; Kothari, D.; Gupta, A.; Gupta, S. Study of weak ferromagnetism in polycrystalline multiferroic Eu doped bismuth ferrite. *Appl. Phys. Lett.* **2009**, *94*, 10–13. [[CrossRef](#)]
- Sando, D.; Barthélémy, A.; Bibes, M. BiFeO₃ epitaxial thin films and devices: Past, present and future. *J. Phys. Condens. Matter.* **2014**, *26*, 473201. [[CrossRef](#)] [[PubMed](#)]
- Flores, S.J.R.; Silva, L.M.A.; Lopez, J.A.R.; Sizov, A.S.; Emelianov, N.A. Influence of the order of layers deposition and annealing temperature on the multiferroic properties of multilayer BiFeO₃-CoFe₂O₄ nanocomposites. *Ferroelectrics* **2019**, *543*, 107–114. [[CrossRef](#)]
- Nazario-Naveda, R.; Rojas-Flores, S.; Juárez-Cortijo, L.; Gallozzo-Cardenas, M.; Díaz, F.N.; Angelats-Silva, L.; Benites, S.M. Effect of x on the Electrochemical Performance of Two-Layered Cathode Materials xLi₂MnO₃–(1–x) LiNi_{0.5}Mn_{0.5}O₂. *Batteries* **2022**, *8*, 63. [[CrossRef](#)]

6. Flores, S.J.R.; Cardenas, M.M.G.; Naveda, R.R.N.; Cortijo, L.A.J.; Yupanqui, M.R.R.; Silva, L.M.A.; Odar, F.E.U. Influence of cobalt ferrite on the magnetoelectric properties of thin films of bismuth ferrite deposited by spin coating. *Matéria* **2020**, *25*, 1. [[CrossRef](#)]
7. Segundo, R.F.; La Cruz-Noriega, D.; Nazario-Naveda, R.; Benites, S.M.; Delfin-Narciso, D.; Angelats-Silva, L.; Díaz, F. Golden Berry Waste for Electricity Generation. *Fermentation* **2022**, *8*, 256. [[CrossRef](#)]
8. Flores, S.R.; Pérez-Delgado, O.; Naveda-Renny, N.; Benites, S.M.; de la Cruz-Noriega, M.; Narciso, D.A.D. Generation of Bioelectricity Using Molasses as Fuel in Microbial Fuel Cells. Environmental Research. *Eng. Manag.* **2022**, *78*, 19–27.
9. Coey, J. *Magnetism and Magnetic Materials*; Cambridge University Press: New York, NY, USA, 2010. [[CrossRef](#)]
10. Costa, L.; Rocha, L.; Cortes, J.; Ramirez, M.; Longo, E.; Simoes, A. Enhancement of ferromagnetic and ferroelectric properties in calcium doped BiFeO₃ by chemical synthesis. *Ceram. Int.* **2015**, *41*, 9265–9275. [[CrossRef](#)]
11. Li, J.; Liu, K.; Xu, J.; Wang, L.; Bian, L.; Xu, F. Structure-Dependent Electrical, Optical and Magnetic Properties of Mn-Doped BiFeO₃ Thin Films Prepared by the Sol-Gel Process. *J. Mater. Sci. Res.* **2013**, *2*, 75–81. [[CrossRef](#)]
12. Montes, G.M.; Perales-Perez, O.; Rentería, B.; Gálvez, M. Tuning of Magnetic Properties in Cobalt-Doped Nanocrystalline Bismuth Ferrite. *MRS Proc.* **2011**, *1368*, 1135. [[CrossRef](#)]
13. Chaudhari, Y.A.; Mahajan, C.M.; Jagtap, P.P.; Bendre, S.T. Structural, magnetic and dielectric properties of nano-crystalline Ni-doped BiFeO₃ ceramics formulated by self-propagating high-temperature synthesis. *J. Adv. Ceram.* **2013**, *2*, 135–140. [[CrossRef](#)]
14. Tang, P.; Kuang, D.; Yang, S.; Zhang, Y. Preparation and enhanced ferromagnetic properties in Co doped BiFeO₃ nanoparticles prepared by sol-gel method. *Ferroelectrics* **2016**, *505*, 123–129. [[CrossRef](#)]
15. Han, J.-T.; Huang, Y.-H.; Wu, X.-J.; Wu, C.-L.; Wei, W.; Peng, B.; Huang, W.; Goodenough, J.B. Tunable synthesis of bismuth ferrites with various morphologies. *Adv. Mater.* **2006**, *18*, 2145–2148. [[CrossRef](#)]
16. Chinchay-Espino, H.; Montes-Albino, G.; Villa-Santos, C.; Perales-Pérez, O. Structural and Magnetic Properties of Pure and Mn-Doped Bismuth Ferrite Powders. *MRS Adv.* **2017**, *2*, 253–258. [[CrossRef](#)]
17. Wang, L.; Xu, J.; Gao, B.; Chang, A.; Chen, J.; Bian, L.; Song, C. Synthesis of BiFeO₃ nanoparticles by a low-heating temperature solid-state precursor method. *Mater. Res. Bull.* **2013**, *48*, 383–388. [[CrossRef](#)]
18. Taylor, P.; Xie, H.; Wang, K.; Jiang, Y.; Zhao, Y.; Wang, X.; Xie, H.; Wang, K.; Jiang, Y.; Zhao, Y.; et al. An Improved Co-precipitation Method to Synthesize Three Bismuth Ferrites. *Synth. React. Inorg. Met.-Org. Nano-Met. Chem.* **2014**, *44*, 1363–1367. [[CrossRef](#)]
19. Zheng, X.; Xu, Q.; Wen, Z.; Lang, X.; Wu, D.; Qiu, T.; Xu, M. The magnetic properties of La doped and codoped BiFeO₃. *J. Alloy. Compd.* **2010**, *499*, 108–112. [[CrossRef](#)]
20. Hasan, M.; Islam, M.; Mahbub, R.; Hossain, M.; Hakim, M. A soft chemical route to the synthesis of BiFeO₃ nanoparticles with enhanced magnetization. *Mater. Res. Bull.* **2016**, *73*, 179–186. [[CrossRef](#)]
21. Kumar, N.S.; Kumar, K.V. Synthesis and Structural Properties of Bismuth Doped Cobalt Nanoferrites Prepared by Sol-Gel Combustion Method. *World J. Nano Sci. Eng.* **2015**, *5*, 140–151. [[CrossRef](#)]
22. Sakar, M.; Balakumar, S.; Saravanan, P.; Jaisankar, S. Annealing temperature mediated physical properties of bismuth ferrite (BiFeO₃) nanostructures synthesized by a novel wet chemical method. *Mater. Res. Bull.* **2013**, *48*, 2878–2885. [[CrossRef](#)]
23. Rout, J.; Choudhary, R.; Sharma, H.; Shannigrahi, S. Effect of co-substitutions (Ca-Mn) on structural, electrical and magnetic characteristics of bismuth ferrite. *Ceram. Int.* **2015**, *41*, 9078–9087. [[CrossRef](#)]
24. Vashisth, B.K.; Bangruwa, J.S.; Beniwal, A.; Gairola, S.P.; Kumar, A.; Singh, N.; Verma, V. Modified ferroelectric/magnetic and leakage current density properties of Co and Sm co-doped bismuth ferrites. *J. Alloy. Compd.* **2017**, *698*, 699–705. [[CrossRef](#)]
25. Chakrabarti, K.; Sarkar, B.; Ashok, V.; de Chaudhuri, S. Enhanced magnetic and dielectric behavior in Co doped BiFeO₃ nanoparticles. *J. Magn. Magn. Mater.* **2015**, *381*, 271–277. [[CrossRef](#)]
26. Mukherjee, A.; Basu, S.; Green, L.; Thanh, N.; Pal, M. Enhanced multiferroic properties of Y and Mn codoped multiferroic BiFeO₃ nanoparticles. *J. Mater. Sci.* **2015**, *50*, 1891–1900. [[CrossRef](#)]
27. Lotey, G.; Verma, N. Structural, magnetic, and electrical properties of Gd-doped BiFeO₃ nanoparticles with reduced particle size. *J. Nanoparticle Res.* **2012**, *14*, 742. [[CrossRef](#)]